Deposition Techniques

DOI: 10.1002/anie.200907168

Low-Temperature ABC-Type Atomic Layer Deposition: Synthesis of Highly Uniform Ultrafine Supported Metal Nanoparticles**

*Junling Lu and Peter C. Stair**

Transition-metal nanoparticles on oxide supports are objects of great interest in heterogeneous catalysis due to their unique chemical and physical properties.[1–4] Ultrafine metal nanoparticles (< 1 nm) with a narrow size distribution grown using mass-selection and soft-landing techniques at low temperature have shown high catalytic activity.[4–8] However, these preparations cannot be applied to high surface area powder supports for practical applications. With conventional preparation methods such as co-precipitation, impregnation, and chemical vapor deposition, metal nanoparticles (> 1 nm) with a broad size distribution are usually formed,[9–11] and ultrafine metal nanoparticles are obtained only at extremely low loadings.[12–14] Alternatively, controlled colloidal synthesis has been developed to control size and size distribution, where the presence of protective ligands prevents metal agglomeration.[14–17] With this method, the metal nanoparticles must still be grafted to catalyst carriers to fabricate supported catalysts, and metal agglomeration must be prevented by coating with one or more monolayers of stabilizing agents, such as polymers.[14,16,17] It remains a challenge to synthesize ultrafine metal nanoparticles with a narrow size distribution on high surface area supports, especially at high loadings.

Atomic layer deposition (ALD) is a thin film growth technique, which relies on self-limiting binary reactions between gaseous precursor molecules and a substrate to deposit uniform films in a layer-by-layer fashion.[18,19] The deposited amount can be precisely controlled simply by tuning the number of deposition cycles. Very recently, a few groups have expanded its application to synthesize both metal and metal oxide catalytic materials.[20–23] The merits of the ALD method for the synthesis of next generation catalysts have been discussed.[24]

Here we report that highly uniform, ultrafine supported metal nanoparticles, regardless of loading, can be directly synthesized on high surface area supports by growing both protected metal nanoparticles and support simultaneously using low temperature, ABC-type atomic layer deposition.

Figure 1 shows a schematic model for this new method. The initial support surface with a number of nucleation sites for metal precursor **A** is shown in Figure 1a. The initial support surface is exposed to **A**, a volatile metal precursor to grow protected metal nanoparticles where a portion of the metal precursor ligands are retained to prevent further agglomeration (Figure 1b). The first reagent **B**, which usually reacts with surface hydroxy groups, is then introduced to the surface (Figure 1c). In the following step, the second reagent **C** is introduced to the surface to react with **B** and form new support surface for the next **A** exposure (Figure 1d). Here the new support forms only on exposed support surfaces not on the protected metal nanoparticles. With sufficient inert gas purging between each precursor exposure, all weakly bound species are removed. After a selected number of ABC cycles are performed, a certain density of protected metal nanoparticles and new support are formed on the initial support (Figure 1e). In the final step, the protective ligands are removed by calcination and/or reduction at elevated temperature to activate the metal nanoparticles (Figure 1f).

There are two key factors required for this new approach to process multiple deposition cycles without covering up the metal particles formed at the initial stages: 1) **B** and **C** must be unreactive with **A**, which allows **A** to remain uncovered even after a number of ABC deposition cycles. 2) **B** and **C** must exhibit self-limiting binary reactions at low temperature to form new support surface for the next **A** exposure in the ABC-type ALD. It should be mentioned that the new support formed during each ABC cycle does not have to be the same material as the initial carrier surface, which allows one to easily grow metal nanoparticles on mixed supports as required by the application.

To explore this synthesis strategy, palladium(II) hexafluoroacetylacetonate, [Pd(hfac)$_2$], was used as the **A** metal precursor, trimethylaluminum (TMA) or titanium isopropoxide (TTIP) was used as the **B** reagent, and water was used as the **C** reagent. It is known that there is no reaction between [Pd(hfac)$_2$] and water at least below 200 °C.[25] Figure 2

[*] Prof. P. C. Stair
Department of Chemistry and Center for Catalysis and Surface Science, Northwestern University
Evanston, IL 60208-4195 (USA)
and
Chemical Sciences and Engineering Division
Argonne National Laboratory
Argonne, IL 60439 (USA)
Fax: (+1) 847-467-1018
E-mail: pstair@northwestern.edu
Homepage: http://chemgroups.northwestern.edu/stair/
Dr. J. Lu
Department of Chemistry and Center for Catalysis and Surface Science, Northwestern University
Evanston, IL 60208-4195 (USA)

[**] This work was financially supported by Dow Chemical Company under Dow methane challenge project. The ALD system construction was funded by DOE (DE-FG02-03ER15457), AFOSR (MURI F49620-02-1-0381, DURIP FA-9550-07-1-0526), and DTRA JSTO FA9550-06-1-0558. The authors thank Jeffrey W. Elam, Jeffrey T. Miller, Neng Guo and Kathryn M. Kosuda for the technical assistance, and David D. Graf, Lin Luo and Harold H. Kung for the constructive discussions.

Supporting information for this article is available on the WWW under http://dx.doi.org/10.1002/anie.200907168.

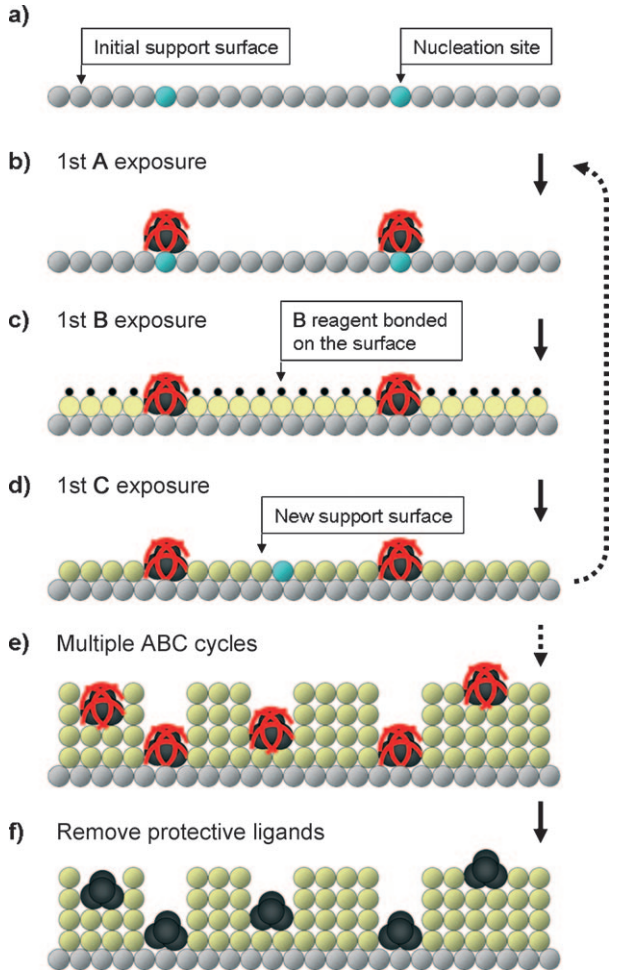

Figure 1. A schematic model of ABC-type ALD: a) An initial support with nucleation sites. b) A volatile metal precursor **A** is introduced to the surface to form metal nanoparticles with part of ligands retained (red curves). c) The first reagent **B** is introduced to the surface. d) The second reagent **C** is introduced to the surface to react with **B** and form a new support surface. e) New support and metal nanoparticles protected by ligands are formed on the initial support surface after multiple ABC cycles. f) The protective ligands are removed to activate metal nanoparticles.

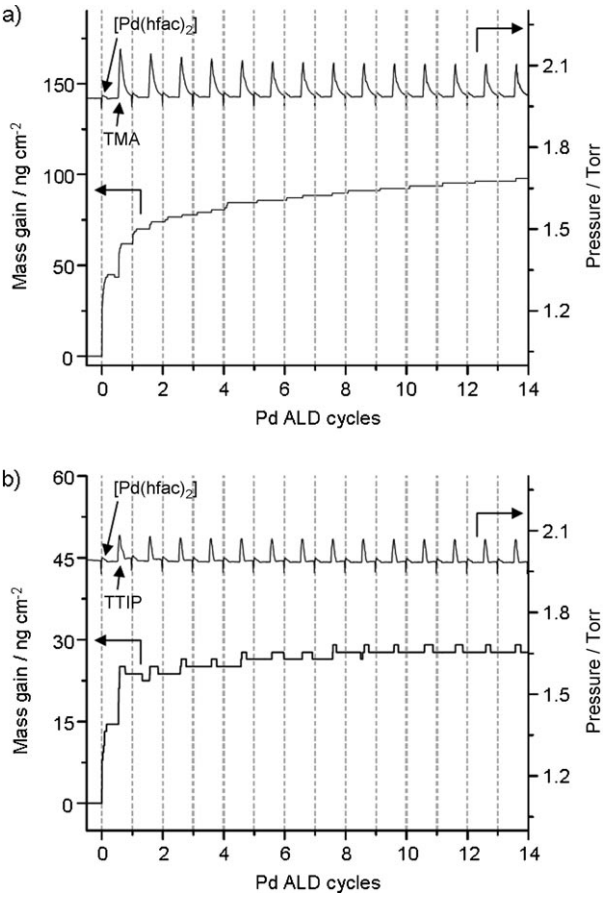

Figure 2. Mass gain and reactor pressure during sequential $[Pd(hfac)_2]$ and TMA or TTIP exposures on the Al_2O_3 or TiO_2 pre-coated QCM, respectively. The mass gain after each $[Pd(hfac)_2]$ exposure is indicated by the dash line: a) First 14 cycles of sequential $[Pd(hfac)_2]$ and TMA exposures at 80 °C (2–10–5–10); b) first 14 cycles of sequential $[Pd(hfac)_2]$ and TTIP exposures at 110 °C (2–10–5–10).

illustrates reactor pressure and quartz crystal microbalance (QCM) mass gain during cycles of the **A** and **B** reagent exposures. It demonstrates that there is essentially no reaction between either $[Pd(hfac)_2]$ and TMA at 80 °C (Figure 2a), or $[Pd(hfac)_2]$ and TTIP at 110 °C (Figure 2b), which is consistent with the literature results.[26] However, a common feature in Figures 2a and b, is the observation of significant mass gain after the first $[Pd(hfac)_2]$ exposure, followed by remarkably decreasing mass gain in subsequent cycles. The significant mass gain after the first $[Pd(hfac)_2]$ exposure demonstrates the key role of the BC steps in the ABC-type ALD process.

Figure 3 shows the mass gain data of ABC-type Pd ALD on both Al_2O_3 and TiO_2: $[Pd(hfac)_2]$ + TMA + H_2O at 80 °C and $[Pd(hfac)_2]$ + TTIP + H_2O at 110 °C. Here the number of Pd ALD cycles is defined by counting the number of $[Pd(hfac)_2]$ exposures. As shown in Figure 3a, the growth corresponding to these two cases was essentially linear. This is very different from AB-type Pd ALD by sequential exposure to $[Pd(hfac)_2]$ and formalin at 200 °C on Al_2O_3, where there is a period of low growth at the beginning of the deposition followed by a stable growth rate of about 0.2 Å/cycle.[25] The details of the growth rate together with the pressure in the deposition chamber for both cases in the stable growth region are shown in Figures 3b and c. After each $[Pd(hfac)_2]$ exposure, the mass gain of protected Pd nanoparticles was about 10.2 ng cm^{-2} for $[Pd(hfac)_2]$ + TMA + H_2O and 2.2 ng cm^{-2} for $[Pd(hfac)_2]$ + TTIP + H_2O. The mass gain on Al_2O_3 was greater than on TiO_2 after each $[Pd(hfac)_2]$ exposure because the formation of new Al_2O_3 support (25.1 ng cm^{-2} per cycle) was much greater than of new TiO_2 support (6.7 ng cm^{-2} per cycle). This result indicates that the growth rate of protected Pd nanoparticles is proportional to the new support surface area created after each **B** + **C** exposure.[27]

For electron microscopy studies, spherical silica gel, overcoated by 10 cycles of Al_2O_3 or TiO_2, was used as a high surface area support to deposit Pd using ABC-type ALD at temperatures of 80 and 110 °C, respectively. Scanning transmission electron microscopy (STEM) shows that protected Pd

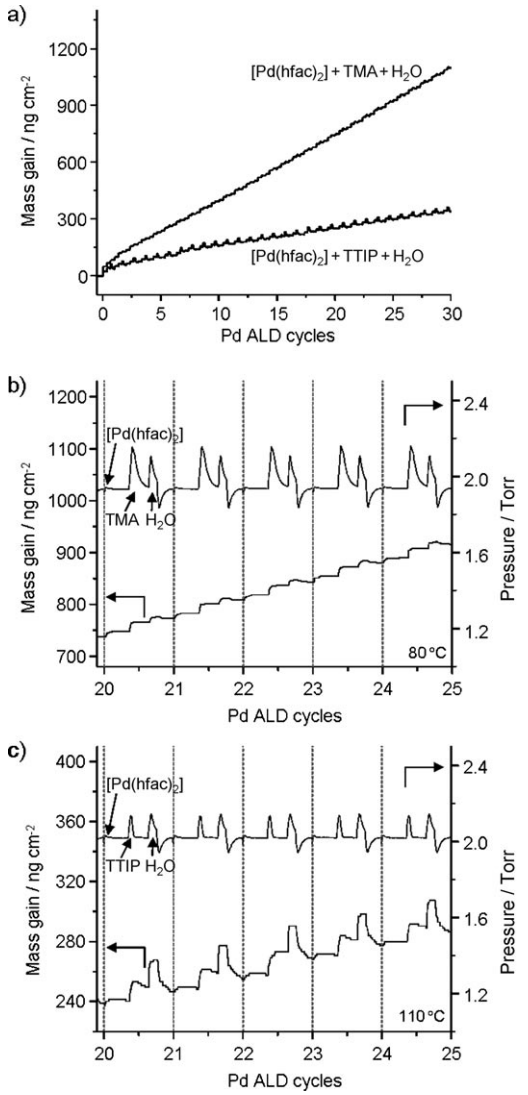

Figure 3. Mass gain and reactor pressure during ABC-type Pd ALD on the Al_2O_3 or TiO_2 pre-coated QCM: a) Mass gain during sequential [Pd(hfac)$_2$], TMA and H_2O exposures on the Al_2O_3 surface at 80 °C and sequential [Pd(hfac)$_2$], TTIP and H_2O exposures on the TiO_2 surface at 110 °C; b) mass gain and reactor pressure in a stable grow region during ABC-type Pd ALD on Al_2O_3 at 80 °C; c) mass gain and reactor pressure in a stable grow region during ABC-type Pd ALD on TiO_2 at 110 °C.

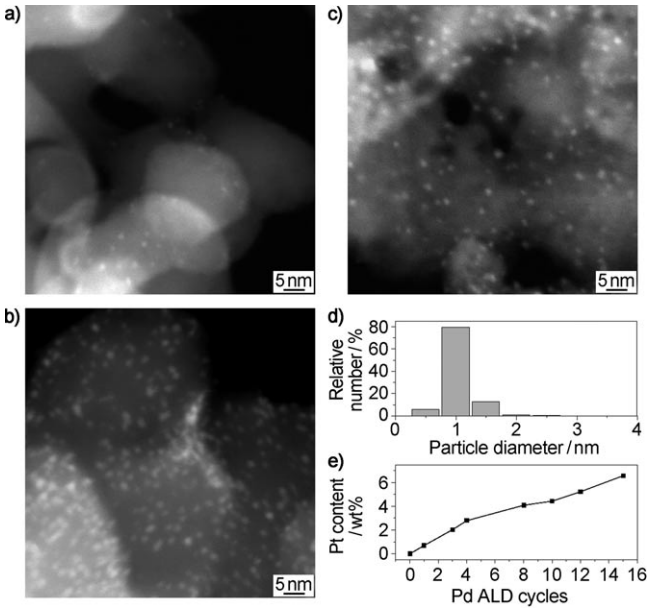

Figure 4. Morphology, size distribution histogram, and weight percentage of as-prepared Pd nanoparticles on high surface area 10-cycle Al_2O_3 coated silica gel support by different cycles of ABC-type Pd ALD at 80 °C: a) STEM image of an as-prepared 1 PdAl–10 AlSi sample, b) STEM image of an as-prepared 4 PdAl–10AlSi sample, c) STEM image of an as-prepared 15 PdAl–10 AlSi sample; d) size distribution histogram of Pd nanoparticles on the as-prepared 15 PdAl–10 AlSi sample; e) Pd content by weight percentage for different Pd ALD cycles on high surface area 10-cycle Al_2O_3 coated silica gel support at 80 °C.

nanoparticles exhibited very high dispersions on the Al_2O_3 support after various numbers of ALD cycles (x PdAl–10 AlSi), (Figures 4 a–c). The Pd particle size was constant at about 1 nm with increasing numbers of deposition cycles in the range 1 to 15, while the density of Pd nanoparticles increased. Figure 4 d shows that the distribution of Pd particle sizes on the 15 PdAl–10 AlSi sample was extremely narrow. Within the 0.3 nm to 2.5 nm range, about 80 % of the Pd nanoparticles had a particle size which differed by not more than 0.2 nm from the average particle size. The Pd loading with different ALD cycles was quantified by inductively coupled plasma atomic emission spectroscopy. The results show that the Pd content (wt %) increased slightly faster for the first four Pd ALD cycles and then exhibited nearly linear growth after ten Pd ALD cycles. The range of loadings was 0.7 % to 6.6 % for the 1 to 15-cycle samples.

Figure 5 shows the STEM image of an as-prepared sample with four ALD cycles of Pd on TiO_2 at 110 °C (4 PdTi–10 TiSi) and the histogram of the Pd particle sizes. The diameter of the ultrafine Pd nanoparticles formed on TiO_2 was about 1 nm with an extremely narrow size distribution in the range of 0.2 nm to 2.2 nm, where about 68 % of the Pd nanoparticles had a particle size which differed by not more than 0.2 nm from the average particle size. Compared with the Pd/Al_2O_3 sample prepared at 80 °C, the fraction of Pd nanoparticles with diameters of about 0.5 nm on TiO_2 increased slightly, consistent with slower diffusion by adsorbed [Pd(hfac)$_2$] and stronger chemical bonding on TiO_2.

DRIFTS studies (diffuse reflectance infrared Fourier transform spectroscopy) of CO chemisorption on the as-prepared samples provides further evidence that protected Pd nanoparticles were formed on the surface from the observation of bridged and three-fold hollow site CO at 1981 and 1926 cm^{-1}, respectively.[27,28] While the mechanism for nucleation and diffusion of [Pd(hfac)$_2$] on the surface to form protected Pd nanoparticles is unclear, it is likely related to reaction between the [Pd(hfac)$_2$] precursor and only certain types of hydroxy groups, since a considerable number of hydroxy groups remain after [Pd(hfac)$_2$] exposure and react with reagent **B** in the ABC cycle.

Here, it should be mentioned that the Pd particle size distribution exhibited by these Pd/Al_2O_3 and Pd/TiO_2 materi-

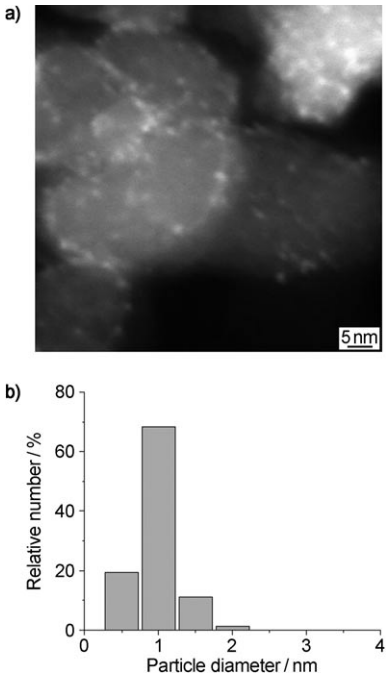

Figure 5. Morphology and size distribution histogram of as-prepared Pd nanoparticles on high surface area 10-cycle TiO_2 coated silica gel support by 4-cycle ABC-type Pd ALD with sequential [Pd(hfac)$_2$], TTIP and H_2O exposures at 110 °C: a) STEM image of an as-prepared 4 PdTi–10 TiSi sample; b) size distribution histogram of Pd nanoparticles on the as-prepared 4 PdTi–10 TiSi sample.

als prepared by the low temperature ABC-type ALD method was significantly narrower than the materials prepared using the traditional AB-type ALD method of exposure to [Pd(hfac)$_2$] and formalin at 200 °C.[25,27] The significantly narrower size distribution resulting from the ABC-type ALD method is a consequence of both the lower reaction temperature which decreases adsorbate diffusion rates and the protective ligands which prevent further agglomeration.

Ultimately, the protective ligands can be simply removed to activate the metal nanoparticles by exposure to formalin at 200 °C for 1 h without changing the size of the Pd nanoparticles.[27] The presence and removal of protective ligands on the as-prepared samples after formalin exposure are indicated by a strong increase in the CO chemisorption capacity. Moreover, the CO chemisorption capacity is proportional to the number of Pd ALD cycles, which indicates that all Pd nanoparticles are accessible.[27]

To the best of our knowledge, this is the first example of directly synthesizing highly uniform ultrafine supported metal nanoparticles on high surface area supports, regardless of loading. There are four advantages in this new approach. 1) It can be achieved at much lower temperature compared with traditional ALD reaction conditions; 2) it can be easily applied to high surface area supports; 3) the density of metal nanoparticles is tunable without varying the size; 4) the size distribution of metal nanoparticles is very narrow. These advantages could make it possible to scale up this novel method for an industrial application with low cost and high performance in catalytic activity and selectivity.

In conclusion, we have shown that highly uniform ultrafine supported Pd nanoparticles, independent of loading, can be directly synthesized on high surface area supports by depositing metal nanoparticles with protective ligands and growing supports sequentially using low temperature ABC-type atomic layer deposition. We believe that this strategy can be extended to other transition metals and supports by the proper combination of volatile metal precursors and **B** + **C** reagents which can react according to a self-limiting process at lower temperature (< 150 °C).[27]

Experimental Section

The Pd ALD was performed using a viscous flow reactor system equipped with a quartz crystal microbalance (QCM), which allows measurement of the growth rate in situ during the ALD process.[29] Ultrahigh purity nitrogen (99.999 %) carrier gas continuously passes through the flow tube reactor at a mass flow rate of 360 sccm and a pressure of 1 to 2 Torr. Trimethylaluminum (TMA, Sigma–Aldrich, 97 %) and millipore water were used to grow Al_2O_3 films. Titanium isopropoxide (TTIP, Sigma–Aldrich, 97 %) and Millipore water were used to grow TiO_2 films, where the TTIP reservoir was heated to 100 °C to achieve sufficient vapor pressure and reasonable dose times.[30] [Pd(hfac)$_2$] (Sigma–Aldrich, > 97 %) contained in a metal precursor bubbler was heated to 60 °C in order to obtain sufficient vapor pressure. In all cases, the inlet lines were heated to at least 100 °C to prevent condensation.

For the traditional AB-type ALD, the ALD timing sequences can be expressed as t_1–t_2–t_3–t_4 where t_1 is the exposure time for the first precursor, t_2 is the purge time following the first exposure, t_3 is the exposure time for the second precursor, t_4 is the purge time following the exposure of the second precursor. All units here are given in seconds (s). In the same way, the ALD timing is t_1–t_2–t_3–t_4–t_5–t_6 for the ABC-type ALD.

To monitor the Pd compound growth rate on Al_2O_3 and TiO_2 supports with ABC-type ALD using in situ QCM, a 1 to 10 nm thick layer of Al_2O_3 or TiO_2 was initially deposited on the surface of the QCM by exposure to TMA and H_2O (2–5–2–5) or TTIP and H_2O (4–5–4–5) for about 100 cycles.[25] Subsequently, ABC-type Pd ALD was performed by exposing either [Pd(hfac)$_2$] + TMA + H_2O (5–10–2–10–5–10) at 80 °C or [Pd(hfac)$_2$] + TTIP + H_2O (5–10–2–10–5–10) at 110 °C.

Spherical silica gel (Silicycle S10040M) with a surface area of about 100 $m^2 g^{-1}$, a primary particle size of 75–200 μm, and a nominal pore diameter of 30 nm was used as an initial substrate. Normally, 200 to 300 mg silica gel uniformly dispersed in a fixed-bed powder holder was loaded into the ALD reactor. Prior to the ABC-type Pd ALD, 10 cycles of Al_2O_3 or TiO_2 were used to coat the silica gel at 177 °C by alternatively exposing TMA and H_2O (50, 150, 200, 200), or at 150 °C by alternatively exposing TTIP and H_2O (60, 240, 120, 240).[30] Then the reactor was cooled down to perform the ABC-type Pd ALD, where the exposure and purge time sequence is 300, 300, 50, 150, 300 and 300 s for [Pd(hfac)$_2$] + TMA + H_2O at 80 °C and 300, 300, 60, 240, 300 and 300 s for [Pd(hfac)$_2$] + TTIP + H_2O at 110 °C. The loading of Pd on the alumina over-coated silica gel was determined by ICP-AES.

Scanning transmission electron microscopy (STEM) measurements were performed on a JEOL JEM-2100F fast transmission electron microscopy system (EPIC facility at Northwestern University) operated at 200 KV.

Received: December 18, 2009
Published online: March 12, 2010

Keywords: atomic layer deposition · low-temperature techniques · metal nanoparticles · palladium · supported catalysts

[1] H. J. Freund, M. Bäumer, H. Kuhlenbeck, *Adv. Catal.* **2000**, *45*, 333 – 384.
[2] C. T. Campbell, *Surf. Sci. Rep.* **1997**, *27*, 1 – 111.
[3] M. Valden, X. Lai, D. W. Goodman, *Science* **1998**, *281*, 1647 – 1650.
[4] U. Heiz, E. L. Bullock, *J. Mater. Chem.* **2004**, *14*, 564 – 577.
[5] S. Abbet, K. Judai, L. Klinger, U. Heiz, *Pure Appl. Chem.* **2002**, *74*, 1527 – 1535.
[6] S. Vajda, M. J. Pellin, J. P. Greeley, C. L. Marshall, L. A. Curtiss, G. A. Ballentine, J. W. Elam, S. Catillon-Mucherie, P. C. Redfern, F. Mehmood, P. Zapol, *Nat. Mater.* **2009**, *8*, 213 – 216.
[7] K. Judai, S. Abbet, A. S. Wörz, U. Heiz, C. R. Henry, *J. Am. Chem. Soc.* **2004**, *126*, 2732 – 2737.
[8] B. Yoon, H. Häkkinen, U. Landman, A. S. Wörz, J. M. Antonietti, S. Abbet, K. Judai, U. Heiz, *Science* **2005**, *307*, 403 – 407.
[9] R. L. Augustine, *Heterogeneous Catalysis for the Synthetic Chemist*, Marcel Dekker, New York, **1996**, pp. 267 – 312.
[10] J. A. Schwarz, C. Contescu, A. Contescu, *Chem. Rev.* **1995**, *95*, 477 – 510.
[11] M. L. Toebes, J. A. van Dillen, Y. P. de Jong, *J. Mol. Catal. A* **2001**, *173*, 75 – 98.
[12] T. Lopez, M. Asomoza, P. Bosch, E. Garciafigueroa, R. Gomez, *J. Catal.* **1992**, *138*, 463 – 473.
[13] Y. Xie, K. L. Ding, Z. M. Liu, R. T. Tao, Z. Y. Sun, H. Y. Zhang, G. M. An, *J. Am. Chem. Soc.* **2009**, *131*, 6648 – 6649.
[14] K. Okamoto, R. Akiyama, H. Yoshida, T. Yoshida, S. Kobayashi, *J. Am. Chem. Soc.* **2005**, *127*, 2125 – 2135.
[15] L. Guczi, A. Horvath, A. Beck, A. Sarkany, *Sci. Technol. Catal. 2002* **2003**, *145*, 351 – 354.
[16] L. C. Chao, R. P. Andres, *J. Colloid Interface Sci.* **1994**, *165*, 290 – 295.
[17] R. Rinaldi, A. D. Porcari, T. C. R. Rocha, W. H. Cassinelli, R. U. Ribeiro, J. M. C. Bueno, D. Zanchet, *J. Mol. Catal. A* **2009**, *301*, 11 – 17.
[18] M. Leskelä, M. Ritala, *J. Phys. Iv* **1999**, *9*, 837 – 852.
[19] R. L. Puurunen, *J. Appl. Phys.* **2005**, *97*, 121301 – 121352.
[20] J. E. Herrera, J. H. Kwak, J. Z. Hu, Y. Wang, C. H. F. Peden, *Top. Catal.* **2006**, *39*, 245 – 255.
[21] S. T. Christensen, J. W. Elam, F. A. Rabuffetti, Q. Ma, S. J. Weigand, B. Lee, S. Seifert, P. C. Stair, K. R. Poeppelmeier, M. C. Hersam, M. J. Bedzyk, *Small* **2009**, *5*, 750 – 757.
[22] J. S. King, A. Wittstock, J. Biener, S. O. Kucheyev, Y. M. Wang, T. F. Baumann, S. K. Giri, A. V. Hamza, M. Bäumer, S. F. Bent, *Nano Lett.* **2008**, *8*, 2405 – 2409.
[23] J. Keränen, A. Auroux, S. Ek, L. Niinisto, *Appl. Catal. A* **2002**, *228*, 213 – 225.
[24] P. C. Stair, *J. Chem. Phys.* **2008**, *128*, 182507 – 182510.
[25] J. W. Elam, A. Zinovev, C. Y. Han, H. H. Wang, U. Welp, J. N. Hryn, M. J. Pellin, *Thin Solid Films* **2006**, *515*, 1664 – 1673.
[26] D. N. Goldstein, S. M. George, *Appl. Phys. Lett.* **2009**, *95*, 143106 – 143108.
[27] See the Supporting Information.
[28] T. Lear, R. Marshall, J. A. Lopez-Sanchez, S. D. Jackson, T. M. Klapötke, M. Bäumer, G. Rupprechter, H. J. Freund, D. Lennon, *J. Chem. Phys.* **2005**, *123*, 174706 – 174718.
[29] J. W. Elam, M. D. Groner, S. M. George, *Rev. Sci. Instrum.* **2002**, *73*, 2981 – 2987.
[30] J. L. Lu, K. M. Kosuda, R. P. Van Duyne, P. C. Stair, *J. Phys. Chem. C* **2009**, *113*, 12412 – 12418.

